Spatial Heterogeneity of Fault Slip and the Radiated Spectra of Ground Motions

Igor A. Beresnev[*1]

ABSTRACT

Kinematic models of simulating earthquake radiation in seismic hazard analysis typically require prescribing the distribution of final slip over the hypothetical fault planes. The spatial spectra of heterogeneous slip affect the frequency spectra of the seismic body waves. The representation integral of elasticity provides a convenient analytical tool by which the relationships between the slip spectra in the wavenumber domain and the wave spectra in the frequency domain can be scrutinized. In the limit of the waves from a small source in the far field, the Fourier spectrum of wave displacement is the spectrum of the slip-rate function multiplied by the spatial slip spectrum representing fault directivity. A popular model for the latter is the *k*-square slip distribution. Classic results prescribe that for a typical ω-square source time function, such multiplication, conversely to a common assumption that the *k*-square slip distribution always leads to the ω-square decay of the high-frequency seismic spectra, can result in the ω^{-4} power-law decay. Such steep fall-off rates are highly unusual in observations, suggesting that the *k*-square heterogeneous slip in certain cases may significantly underpredict the realistic high-frequency ground motions, including peak velocities and accelerations. An alternative use of heterogeneous slip distributions would be to explain the additional high-frequency diminution of the observed spectra that is usually attributed to ad hoc cutoff ("f_{max}" or "kappa") filters. The simple asymptotic relationships between heterogeneous fault slip and body wave spectra may not hold true in the vicinity of large earthquakes, at distances of main interest to hazard calculations.

KEY POINTS

- How does the variable slip distribution on rupturing faults affect the spectra of radiated body waves?
- The frequency spectrum of waves is the spectrum of slip-rate function multiplied by the spatial slip spectrum.
- The commonly assumed k^{-2} slip distribution may significantly underpredict the realistic ground motions.

INTRODUCTION

Prescribing fault-slip distributions for the kinematic models of earthquake radiation is an important component of modern seismic hazard assessment (Somerville *et al.*, 1999; Mai and Beroza, 2002; Graves and Pitarka, 2010, 2016; Schmedes *et al.*, 2013; Infantino *et al.*, 2020; Rodgers *et al.*, 2020; Razafindrakoto *et al.*, 2021). In assessing the impact of various slip distributions on the resulting ground motions, it is useful to acquire general understanding of the relationships between the spatial characteristics of slip and the frequency spectra of radiation. Developing such an understanding is not new; however, there is still a practical need in general relationships highlighting the main controls exerted by the spatial spectra of slip on the radiated waves. In our view, misconceptions exist that could be readily revealed and corrected by such relationships.

A convenient and accurate tool that can be used for this purpose is the representation integral of elasticity, which prescribes the exact wavefield emitted by a displacement discontinuity across a fault plane in a homogeneous elastic space. The full form of the integral can be used for the near field, as well as its asymptotic forms for small sources and large distances. Summarizing specific inferences from such an analysis has both instructional and practical value.

In the following, to better tease out the effects of variable slip on seismic radiation, we will assume the velocity of rupture propagation to be constant. The phenomena arising from variable rupture speed have been addressed in two separate articles (Beresnev, 2021; Beresnev and Roxby, 2021). The conclusions have been twofold. First, variable speed does not

1. Department of Geological and Atmospheric Sciences, Iowa State University, Ames, Iowa, U.S.A., https://orcid.org/0000-0002-4050-919X (IAB)

*Corresponding author: beresnev@iastate.edu

Cite this article as Beresnev, I. A. (2022). Spatial Heterogeneity of Fault Slip and the Radiated Spectra of Ground Motions, *Bull. Seismol. Soc. Am.* **112**, 1463–1471, doi: 10.1785/0120210235

necessarily lead to the enhancement in high-frequency radiation. Radiation from orderly (nonrandomized) changes in the velocity is fully controlled by the interference effects and can be above or below the levels produced by constant rupture speed. Randomizing the velocity destroys the patterns of regular interference and eliminates the artifacts of suppressing the high-frequency levels by destructive interference. Randomization does not in itself enhance the high-frequency levels; if it does, this is through the elimination of artifacts. Hisada (2000) shows similar patterns; the more regular the rupture time becomes, the faster the high-frequency slope of radiated spectra decays (compare fig. 4 of Beresnev and Roxby, 2021 for a finite-fault rupture or fig. 2 of Beresnev, 2019b for a line source with fig. 6a,b of Hisada, 2000). Second, randomization substantially reduces the difference between the forward and reverse directivity pulses.

FULL SPECTRUM OF FAULT RADIATION

Aki and Richards (1980, their equation 14.37) and Beresnev (2017b, his equation 1) provide the full form of the representation integral. Assume a source time (slip) function in the form of a radially propagating rupture,

$$\Delta u(\boldsymbol{\xi}, t) = U(\boldsymbol{\xi})\Delta u_s(\boldsymbol{\xi}, t - r/v), \tag{1}$$

in which $U(\boldsymbol{\xi})$ is the distribution of final-slip values over the fault plane, $\Delta u_s(\boldsymbol{\xi}, t)$ is a dimensionless shape function, $r = |\boldsymbol{\xi} - \boldsymbol{\xi}_0|$, $\boldsymbol{\xi}_0$ is the hypocenter location, and v is the rupture propagation speed, which can be a function of $\boldsymbol{\xi}$. Then, the application of the Fourier transform to the integral leads to the radiated frequency spectrum of the displacement component $u_i(\mathbf{x}, t)$ of the wavefield at the observation point $\mathbf{x}$ (Beresnev, 2017a, his equation 4):

$$\begin{aligned} u_i(\mathbf{x}, \omega) = {} & \frac{\mu}{4\pi\rho}\Delta u_s(\omega) \\ & \times \iint U(\boldsymbol{\xi}) e^{-i\omega\frac{r}{v}} \left[\frac{30\gamma_i n_p \gamma_p \gamma_q v_q - 6\nu_i n_p \gamma_p - 6 n_i \gamma_q v_q}{R^4} t_1(\omega) \right. \\ & + \frac{12\gamma_i n_p \gamma_p \gamma_q v_q - 2\nu_i n_p \gamma_p - 2 n_i \gamma_q v_q}{\alpha^2 R^2} e^{-i\omega\frac{R}{\alpha}} \\ & - \frac{12\gamma_i n_p \gamma_p \gamma_q v_q - 3\nu_i n_p \gamma_p - 3 n_i \gamma_q v_q}{\beta^2 R^2} e^{-i\omega\frac{R}{\beta}} \\ & + \frac{2\gamma_i n_p \gamma_p \gamma_q v_q}{\alpha^3 R} i\omega e^{-i\omega\frac{R}{\alpha}} \\ & \left. - \frac{2\gamma_i n_p \gamma_p \gamma_q v_q - \nu_i n_p \gamma_p - n_i \gamma_q v_q}{\beta^3 R} i\omega e^{-i\omega\frac{R}{\beta}} \right] d\Sigma(\boldsymbol{\xi}). \end{aligned} \tag{2}$$

Here, $\Delta u_s(\omega)$ is the Fourier transform of $\Delta u_s(t)$, in which we have assumed that the temporal function $\Delta u_s(t)$ does not depend on the position on the fault plane, allowing us to factor $\Delta u_s(\omega)$ out of the integral. In addition, $\mathbf{n}$ is the unit vector in the direction of slip, $\boldsymbol{\nu}$ is the unit normal to the fault, $R = |\mathbf{x} - \boldsymbol{\xi}|$, $\boldsymbol{\gamma} = (\mathbf{x} - \boldsymbol{\xi})/R$, α and β are the P- and S-wave propagation speeds, and μ and ρ are the shear modulus and density of the medium, respectively. The integration in equation (2) is over the fault plane. The function $t_1(\omega)$ in the integrand is

$$t_1(\omega) = \frac{1}{\omega}\left[e^{-i\omega\frac{R}{\beta}}\left(i\frac{R}{\beta} + \frac{1}{\omega} \right) - e^{-i\omega\frac{R}{\alpha}}\left(i\frac{R}{\alpha} + \frac{1}{\omega} \right) \right]. \tag{3}$$

Equation (2) shows that the spectrum of the seismic field is that of the source time function $\Delta u_s(\omega)$ modified by the integral $\mathbf{I}(\mathbf{x}, \omega)$ over the fault representing the fault's directivity pattern,

$$\mathbf{u}(\mathbf{x}, \omega) = \Delta u_s(\omega)\mathbf{I}(\mathbf{x}, \omega). \tag{4}$$

We can refer to $\mathbf{I}(\mathbf{x}, \omega)$ as the directivity spectrum. In general case, it is a function of complicated form. The presence of $\mathbf{I}(\mathbf{x}, \omega)$ as the surface integral in equation (2) is purely due to the fault finiteness and the resulting interference effects specific to fault geometry. When the source dimensions shrink to a point, all distance-dependent factors are taken out of the integral, and $u_i(\mathbf{x}, \omega)$ converges to the classic expression for the radiation from a point shear dislocation (Aki and Richards, 1980, their equation 4.32).

It should be remembered that, in the case of fault-position-dependent temporal function $\Delta u_s(\boldsymbol{\xi}, t)$, it will not be possible to factor its spectrum out of the integral in equation (2), and the spectrum $\Delta u_s(\boldsymbol{\xi}, \omega)$ will appear as a multiplier of $U(\boldsymbol{\xi})$ in front of the brackets in the integrand.

SPECTRUM FROM A SMALL SOURCE IN THE FAR FIELD

Equation (2) significantly simplifies and acquires transparent meaning in the limiting case of a small source radiating into the far field. For the general case of fault-position-dependent $\Delta u(\boldsymbol{\xi}, t)$, the respective asymptotic form of equation (2) for shear-wave radiation is given by equation (14.14) of Aki and Richards (1980):

$$\begin{aligned} u_i(\mathbf{x}, \omega) = {} & -\mu \frac{2\gamma_i n_p \gamma_p \gamma_q v_q - \nu_i n_p \gamma_p - n_i \gamma_q v_q}{4\pi\rho\beta^3 r_0} e^{i\omega\frac{r_0}{\beta}} \\ & \times \iint \Delta\dot{u}(\boldsymbol{\xi}, \omega) e^{-i(\mathbf{k}\cdot\boldsymbol{\xi})} d\Sigma, \end{aligned} \tag{5}$$

in which r_0 is the distance to the receiver from the origin (Aki and Richards, 1980, their fig. 14.1), and $\Delta\dot{u}(\boldsymbol{\xi}, \omega)$ is the Fourier spectrum of the time derivative of $\Delta u(\boldsymbol{\xi}, t)$ (the slip velocity) (the dot product is intended in the power of the exponent). The constant vector $\mathbf{k}$ is given by:

$$\mathbf{k} = (\omega/\beta)\boldsymbol{\gamma}, \tag{6}$$

in which $\boldsymbol{\gamma}$ is the unit vector pointing from the origin to the receiver. Aki and Richards (1980) omit the dimensional coefficient in front of the integral in equation (5), which we have retained for completeness. Equation (5) is valid for any general functional form $\Delta u(\boldsymbol{\xi}, t)$ without restricting the rupture to propagate along the fault plane according to the delayed argument in equation (1). It should also be clarified that equation (2) was derived following the traditional sign convention in the Fourier transform on a function of time, in which the sign of the power of the exponent is negative, for example, $f(\omega) = \int_{-\infty}^{\infty} f(t) \exp(-i\omega t) dt$ (Båth, 1974, his section 2.2.2, his equation 20). However, all equations related to the far-field asymptotics of spectra of Aki and Richards (1980), which we are referring to, use the convention in which the sign is positive (Aki and Richards, 1980, p. 87). The moduli of the spectra, for example, those that will be plotted subsequently, are not affected by this difference.

For the fault-position-independent $\Delta u_s(t)$, the slip-rate spectrum $\Delta \dot{u}_s(\omega)$ is taken out of the integral, transforming equation (5) into

$$u_i(\mathbf{x}, \omega) = \text{const} \Delta \dot{u}_s(\omega) \iint U(\boldsymbol{\xi}) e^{-i(\mathbf{k}\cdot\boldsymbol{\xi})} d\Sigma, \tag{7}$$

in which the dimensional coefficient in equation (5) has been designated as a constant. Equation (7) can be rewritten as

$$\begin{aligned} u_i(\mathbf{x}, \omega) &= \text{const} \Delta \dot{u}_s(\omega) U(k_1, k_2) \\ &= \text{const} \Delta \dot{u}_s(\omega) U\left(\frac{\omega}{\beta}\gamma_1, \frac{\omega}{\beta}\gamma_2\right), \end{aligned} \tag{8}$$

in which we have recognized that the double integral in equation (7) is the 2D spatial Fourier transform of the distribution of static slip $U(\boldsymbol{\xi})$ over the fault plane (the spatial slip spectrum in the wavenumber domain), taken, as seen from equation (6), at the specific wavenumbers $k_1 = (\omega/\beta)\gamma_1$ and $k_2 = (\omega/\beta)\gamma_2$ (the spatial transform of U is recognized by its arguments). The directivity spectrum in equation (4) is thus reduced to $I_i(\mathbf{x}, \omega) = \text{const}(-i\omega) U(\omega\gamma_1/\beta, \omega\gamma_2/\beta)$.

The conclusion drawn from equation (8) is that the Fourier spectrum of the far-field displacement is the spectrum of the slip-rate function $\Delta \dot{u}_s(\omega)$ modulated by the multiplication by the spatial slip spectrum representing the fault's directivity.

SPECTRUM FROM A LINE SOURCE

The result in equation (8) can be further simplified in the asymptotics of a near-line source, in which one dimension (e.g., the down-dip width W of the fault) is significantly shorter than the other (e.g., the length L along strike). The respective result for a rupture with constant static slip moving with constant speed is contained in equation (14.18) of Aki and Richards (1980). We generalize it by allowing the static slip to vary as $U(\boldsymbol{\xi})$, according to equation (1), while keeping $\Delta u_s(t)$ as fault-position independent as in the approximation equation (14.18). The beginning of equation (14.18) is then rewritten as

$$\begin{aligned} u_i(\mathbf{x}, \omega) &= -i\omega W \Delta u_s(\omega) \text{const} \int_0^L U(\xi_1) \exp\left[i\omega\xi_1\left(\frac{1}{v} - \frac{\cos\Psi}{\beta}\right)\right] d\xi_1 \\ &= \text{const} W \Delta \dot{u}_s(\omega) U\left[\omega\left(\frac{\cos\Psi}{\beta} - \frac{1}{v}\right)\right], \end{aligned} \tag{9}$$

in which ξ_1 is the distance along the length of the fault, and Ψ is the angle between the direction to the receiver and the ξ_1 axis. The dimensional constant, omitted by Aki and Richards (1980), has again been restored for completeness; it is the same as in equation (7). We have again recognized that the integral in equation (9) is the 1D spatial Fourier transform of $U(\xi_1)$ taken at the wavenumber $\omega(\cos\Psi/\beta - 1/v)$.

The result in equation (9) is equivalent to equation (8) for the case of a line fault and a rupture moving with constant speed. The conclusion we draw remains the same: the Fourier spectrum of the far-field displacement is the spectrum of the slip-rate function modified by the slip spectrum.

SPECTRUM FROM A LINE SOURCE VERSUS EQUIVALENT RESULT OF HERRERO AND BERNARD

The displacement spectrum in equation (9) can be directly contrasted with the often cited equivalent result of Herrero and Bernard (1994). For the same line source approximation, their equation (24) (also reproduced in their Abstract) expresses the far-field frequency spectrum for the fault slip that instantaneously reaches its full value as (our notation is kept for the spectra):

$$u_i(\mathbf{x}, \omega) = FU\left(k_1 = \frac{1}{C_d}\frac{\omega}{v}\right), \tag{10}$$

in which F is a dimensional coefficient not specified by Herrero and Bernard (1994). Considering that $C_d = 1/[1 - (v/\beta)\cos\Psi]$, equation (10) is recast as

$$u_i(\mathbf{x}, \omega) = FU\left[\omega\left(\frac{1}{v} - \frac{\cos\Psi}{\beta}\right)\right]. \tag{11}$$

Comparing with equation (9), one can see that the result of equation (11) in Herrero and Bernard (1994) is incomplete for any realistic fault slip. It is only true for the limiting case in which the slip velocity is the delta function having the unit spectrum. This is never the case. For all practically relevant situations, to obtain the frequency spectrum of the far-field seismic wave, the wavenumber spectrum of slip must be multiplied by the frequency spectrum of the slip-rate function; however, the latter is missing from equation (11). Because such functions typically represent low-pass filters, the multiplication will generally increase the high-frequency slope of the Fourier spectrum of radiation.

MODIFICATION OF THE SPECTRUM OF SOURCE TIME FUNCTION BY SLIP HETEROGENEITY

For a point source, the amplitude spectrum of the far-field displacement is the same as that of the slip-rate function:

$$|u_i(\mathbf{x},\omega)| = \frac{\langle R_{\theta\varphi}\rangle \mu WLU}{4\pi\rho\beta^3 r_0}|\Delta\dot{u}_s(\omega)|, \tag{12}$$

in which r_0 is the distance from the source, U is the average slip, and $\langle R_{\theta\varphi}\rangle$ is the point-source shear-wave angular radiation pattern (Aki and Richards, 1980, their equations 4.32–4.33; Beresnev and Atkinson, 1997, their equation 11).

For a finite source, the slip-rate spectrum is modified by the directivity according to equation (4). We will consider the line source example to illustrate such modification, in which case the resulting frequency spectrum of the seismic wave is given by equation (9). A popular model for the wavenumber spectrum $U(k_1, k_2)$ is the "k^{-2}" ("k-square") slip distribution, introduced by Herrero and Bernard (1994). This model has often been used in the synthetic rupture-slip generators for seismic hazard computations (Somerville *et al.*, 1999, pp. 75–76; Graves *et al.*, 2008; Graves and Pitarka, 2010, p. 2096, 2016; Schmedes *et al.*, 2013, p. 1121; Rodgers *et al.*, 2019; Infantino *et al.*, 2020, pp. 2563–2564; Rodgers *et al.*, 2020, p. 2866; Razafindrakoto *et al.*, 2021). For the line source ($k_2 = 0$), it takes the following form:

$$|U(k_1)| = \begin{cases} C\frac{\Delta\sigma}{\mu}\frac{1}{k_1^2}, & k_1 \geq \frac{1}{L} \\ UL, & k_1 < \frac{1}{L} \end{cases}, \tag{13}$$

in which $\Delta\sigma$ is the mean stress drop, and C is an unspecified geometrical factor ($C \approx 1$) (Herrero and Bernard, 1994, their equation 6 for $k_1 \geq 1/L$ and equation 1 for $k_1 < 1/L$). The low-frequency limit UL has been obtained as $U(k_1 = 0) = \int_0^L U(\xi_1)d\xi_1 = UL$. In modifying equation (13) relative to equation (6) of Herrero and Bernard (1994), the fact has been taken into account that the dimension of the spatial spectrum for the line source, relative to that for a 2D fault plane, is reduced from two to one.

Substitution $k_1 = \omega(\cos\Psi/\beta - 1/v)$ is then made in equation (13), according to equation (9). We note that the resulting conditions $k_1 \geq 1/L$ or $k_1 < 1/L$ in equation (13) cease to make strict sense, because k_1 in the substitution can be negative, which reveals a somewhat artificial character of the k-square spatial spectrum. To circumvent this difficulty in plotting the resulting frequency spectra, albeit arbitrarily to some degree, the condition can be rewritten for the modulus of k_1, introducing the frequency $f_0 = |2\pi L(\cos\Psi/\beta - 1/v)|^{-1}$. The two frequency ranges, corresponding to the two wavenumber ranges in equation (13), will then be $f \geq f_0$ and $f < f_0$.

For the slip-rate spectrum $\Delta\dot{u}_s(\omega)$ in equation (9), we can choose the often used ω-square shape. The amplitude frequency spectrum of the seismic wave, caused by the k-square slip distribution on a line source with the ω-square source time function then becomes, from equation (9),

$$|u_2(\mathbf{x},\omega)| = \begin{cases} \frac{\mu}{4\pi\rho\beta^3 r_0} WC\frac{\Delta\sigma}{\mu}\frac{1}{1+(\frac{\omega}{\omega_c})^2}\frac{1}{\omega^2(\frac{\cos\Psi}{\beta}-\frac{1}{v})^2}, & f \geq f_0 \\ \frac{\mu}{4\pi\rho\beta^3 r_0} WLU\frac{1}{1+(\frac{\omega}{\omega_c})^2} & f < f_0 \end{cases}, \tag{14}$$

in which the explicit value of the quantity $|\text{const}| = \frac{\mu}{4\pi\rho\beta^3 r_0}$ for $\Psi = 0$ (radiation along the direction of rupture propagation) for the fault-normal component ($i = 2$) and the geometry of a vertical right-lateral strike-slip fault (Beresnev, 2021, his equation 7) has been substituted, and ω_c is the corner frequency of the ω-square spectrum of the slip function.

For comparison, we can also take the case in which the slip is constant across the entire fault plane. The spatial spectrum in equation (9) then reduces to the sinc function (Aki and Richards, 1980, their equation 14.18). The resulting equation for radiation, equivalent to equation (14), is

$$|u_2(\mathbf{x},\omega)| = \frac{\mu}{4\pi\rho\beta^3 r_0} WLU\frac{1}{1+(\frac{\omega}{\omega_c})^2}\left|\frac{\sin X}{X}\right|, \tag{15}$$

in which $X = (\omega L/2)[1/v - (\cos\Psi)/\beta]$.

To produce a numerical example of how the original ω-square slip spectrum is modified by the fault directivity resulting from both the k-square and constant slip distributions, we take the following values of the parameters: $\beta = 5000/\sqrt{3}$ m/s, $\rho = 2700$ kg/m^3, $v = 0.8\beta$, and $\Psi = 0$. The parameters $C = 1$, $\Delta\sigma = 4$ MPa, and $\mu = 3.3 \times 10^{10}$ N/m^2 have been borrowed from figure 1 of Herrero and Bernard (1994).

The examples are produced for the characteristic fault dimensions L = 3400 and 10,000 m, corresponding approximately to M_w 5 and 6 earthquakes according to the empirical relationship between the rupture area and the moment magnitude of Wells and Coppersmith (1994, their table 2A). To comply with the condition for the near-line-source approximation ($W \ll L$), the width W is set to 100 m. The respective average offsets U = 0.14 and 0.49 m are calculated as $U = M_0/(\mu A)$, in which the seismic moment M_0 is obtained from the moment magnitude and the fault area A from the equation of Wells and Coppersmith (1994). The frequencies f_0 in the examples are 0.54 and 0.18 Hz for the M_w 5 and 6 events, respectively.

The corner frequency of the ω-square slip for the M_w 5 event was set to a typical value of $f_c = 1$ Hz. This frequency is reduced to the value of 0.30 Hz for M_w 6 in the same proportion as the offsets U used for the two magnitudes, according to equation (18) for the corner frequency discussed subsequently.

The most restrictive of the conditions on the distance to the observation point leading to the small-source approximation in equations (8) and (9) is

$$r_0 \gg \frac{2L^2}{\lambda}, \tag{16}$$

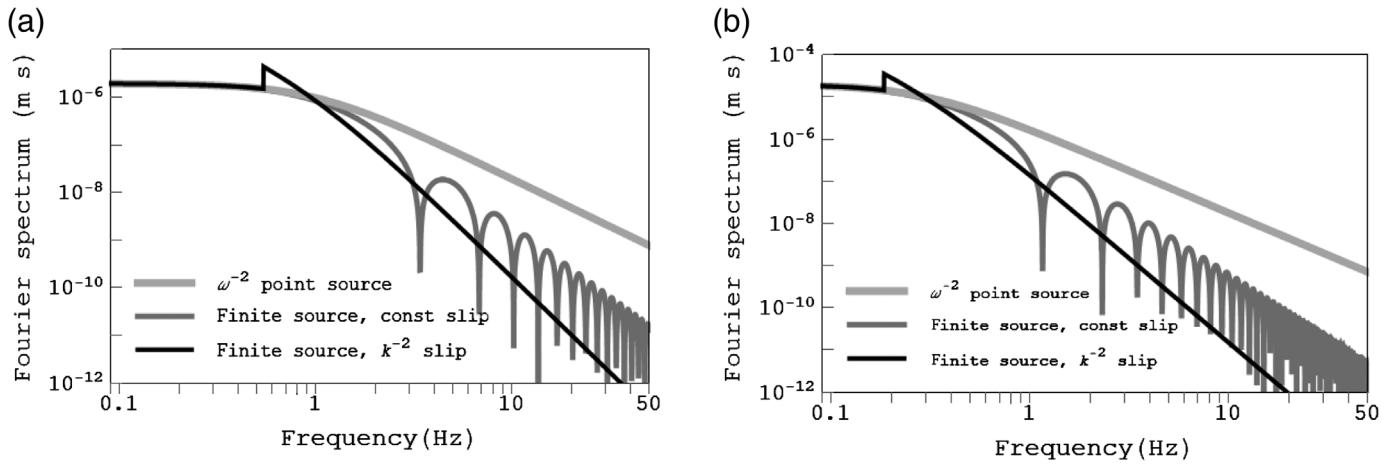

Figure 1. Amplitude spectra of shear-wave radiation from a point shear dislocation, line source with the constant slip, and line source with the k-square slip. All are for the fault-position-independent slip-rate function $\Delta\dot{u}_s(t)$. The values of the high-frequency slopes are −2, −3, and −4. (a) M_w 5 and (b) M_w 6.

in which λ is the wavelength (Aki and Richards, 1980, their equation 14.12). Using L = 3400 m and $\lambda = \beta/50$ m (at the frequency of 50 Hz), we obtain the limits of applicability of equation (9) as $r_0 \gg 400$ km. Accordingly, r_0 will be set to 1000 km. As seen from equations (12), (14), and (15), its specific value does not carry particular significance and merely serves as a scaling factor. This distance is unchanged for the M_w 6 example.

The light gray lines in Figure 1a,b represent the Fourier amplitude spectra of shear-wave radiation from the original point-source ω-square shear dislocation, calculated from equation (12), in which $|\Delta\dot{u}_s(\omega)| = 1/[1 + (\omega/\omega_c)^2]$. The quantity $\langle R_{\theta\varphi}\rangle$ is equal to unity in the direction parallel to the slip vector, as in the example. The dark gray lines are the spectra emitted by the line source with the same ω-square source time function, which is modified by the directivity taken for the constant offset across the fault, computed from equation (15). Finally, the black lines are the same line source spectra radiated by the k-square slip distribution (equation 14). The k^{-2} source radiation has the steepest rate of high-frequency decay, proportional to ω^{-4}, as seen from equation (14). It thus can create a significant deficit in the simulated high-frequency energy. Alternatively, an appropriately chosen heterogeneous slip distribution can explain the much steeper frequency decay of observed spectra than one obtained from point-source modeling. Ad hoc high-cut filtering is required to account for the additional diminution of spectra, termed "$f_{\max}$" or "kappa" filtering, which typically is attributed to local site effects (Boore, 2003, his equations 19 and 20). The same diminution can be explained by pure source effect, owing to the fault finiteness.

It is often argued that the k^{-2} slip distribution results in the ω^{-2} spectral shape of the shear-wave radiation (e.g., Somerville *et al.*, 1999, p. 76; Mai and Beroza, 2002, p. 10–1). This result is typically attributed to the formulation by Herrero and Bernard (1994), in which it can be traced to their equation (24), and the text under it (pp. 1223–1224) that states that "a power-law decay (in wavenumber) for the slip spectrum produces the same power-law decay (in frequency) for the body wave radiation." However, as indicated earlier, equation (24) in Herrero and Bernard (1994) is only valid for the hypothetical situation of instantaneous slip on the entire fault and is thus incomplete. The slip spectrum must be multiplied by the frequency spectrum $\Delta\dot{u}_s(\omega)$ of the slip-rate function to obtain the frequency spectrum of the body wave (equation 9). Equation (9) immediately follows from the classic relationships for the far-field radiation from a small earthquake source. It should be noted that Ruiz *et al.* (2011, their equation 6) do later provide the correct general form of the equation.

SPECTRUM FROM A LINE SOURCE WITH FAULT-POSITION-DEPENDENT SOURCE TIME FUNCTION

A more general form of the slip-rate function is $\Delta\dot{u}(\xi_1, t) = U(\xi_1)\Delta\dot{u}_s(\xi_1, t)$, in which the shape factor $\Delta\dot{u}_s(\xi_1, t)$ varies across the fault. This would be the case, for example, for the slip that produces exactly the ω-square radiated spectrum,

$$\Delta\dot{u}_s(\xi_1, t) = \frac{t}{\tau^2} e^{-t/\tau}, \tag{17}$$

$$\tau = \frac{U(\xi_1)}{e v_{\max}(\xi_1)}, \tag{18}$$

in which $v_{\max}$ is the maximum velocity at which the fault at a point slips, and $\omega_c \equiv 1/\tau$ (Beresnev and Atkinson, 1997, their equation 8; Beresnev, 2001, his equation 3). Although we previously set the corner frequency to a constant value, generally it will be dependent on the local offset and the peak slip rate according to equation (18). The value of τ sets the slip rise time.

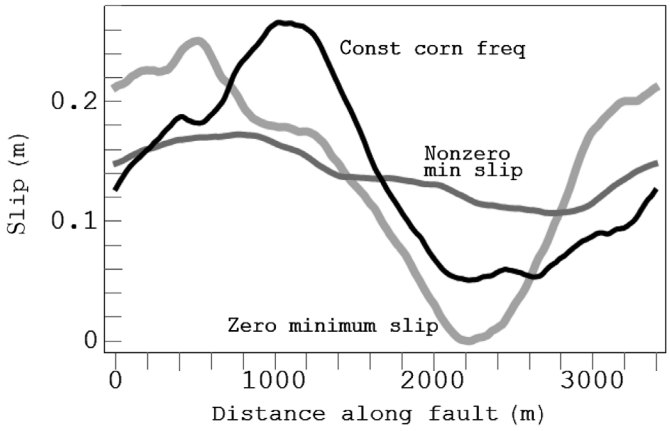

Figure 2. Distributions of slip along the fault line in three different cases used in the calculations through the generalized equation (19).

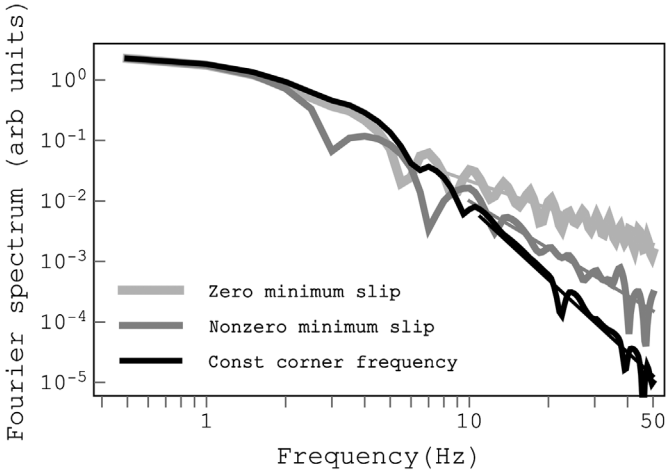

Figure 3. Amplitude spectra of shear-wave radiation from the line source with the slip distributions corresponding to Figure 2. The values of the high-frequency slopes are approximately −1.5, −2.6, and −4. The units on the vertical axis are arbitrary.

The generalized equivalent of equation (9) then becomes

$$u_i(\mathbf{x},\omega) = W\text{const}\int_0^L U(\xi_1)\Delta\dot{u}_s(\xi_1,\omega)\exp\left[i\omega\xi_1\left(\frac{1}{v}-\frac{\cos\Psi}{\beta}\right)\right]d\xi_1$$
$$= \text{const}\,WF\left[\omega\left(\frac{\cos\Psi}{\beta}-\frac{1}{v}\right)\right], \quad (19)$$

in which $F(\xi_1,\omega)\equiv U(\xi_1)\Delta\dot{u}_s(\xi_1,\omega)$, and $F[\omega(\cos\Psi/\beta-1/v)]$ is the spatial spectrum of $F(\xi_1,\omega)$ taken at the wavenumber $\omega(\cos\Psi/\beta-1/v)$. Unlike equation (9), the spatial spectrum now is calculated not for the slip $U(\xi_1)$ but for the product $U(\xi_1)\Delta\dot{u}_s(\xi_1,\omega)$. The complex Fourier spectrum of equation (17) is

$$\Delta\dot{u}_s(\xi_1,\omega) = 1/(1+i\omega\tau)^2. \quad (20)$$

Given equation (18), the spatial spectrum in equation (19) should therefore be calculated for the product $U(\xi_1)/\{1+i\omega U(\xi_1)/[ev_{\max}(\xi_1)]\}^2$. If $U(\xi_1)$ has a complex k-square wavenumber spectrum, the spatial spectrum of the product will be the convolution of this k-square spectrum and the wavenumber spectrum of $\{1+i\omega U(\xi_1)/[ev_{\max}(\xi_1)]\}^{-2}$, in which the functions $U(\xi_1)$ and $v_{\max}(\xi_1)$ must be specified. The simple spectral transformations exemplified in Figure 1 will no longer apply.

An example is provided in Figures 2 and 3, for the same fault and observation point geometry as in the example of Figure 1a. The function $U(\xi_1)$ was generated as follows. The discrete k-square amplitude spectrum was first obtained in the same manner as for Figure 1, for the spatial sampling interval of $\Delta\xi_1 = 10$ m, through

$$|U(k_1)| = \begin{cases} \frac{\mu}{4\pi\rho\beta^3 r_0} WC\frac{\Delta\sigma}{\mu}\frac{1}{k_1^2}, & k_1 \geq \frac{1}{L} \\ \frac{\mu}{4\pi\rho\beta^3 r_0} WLU, & k_1 < \frac{1}{L} \end{cases}. \quad (21)$$

The phase was randomly drawn from the uniform distribution between $-\pi$ and π, as in Graves and Pitarka (2010, their equation A3). The resulting complex spectrum was inverted to produce $U(\xi_1)$, whose real part was taken. If the minimum of the resulting slip distribution was less than zero, it was subtracted to eliminate negative slip, in which case the minimum value became zero. Next, the function $U(\xi_1)$ was renormalized by multiplying it by $U/\bar{U}(\xi_1)$, in which $\bar{U}(\xi_1)$ is the average, to offset the scaling introduced by the discrete inverse Fourier transform and ensure the correct value of the average slip $U = 0.14$ m for the target earthquake.

The function $v_{\max}(\xi_1)$ was generated by adding a normally distributed random number with zero mean and standard deviation of 0.3 m/s to the value of $v_{\max} = 1$ m/s. The velocity was constrained to equal 0.05 and 3 m/s if it accidentally fell below zero or above 3 m/s, respectively. The resulting spatial distribution of $v_{\max}$ was smoothed by a five-point running average, to obtain the overall range of change in $v_{\max}$ from approximately 0.7–1.4 m/s.

The wavenumber spectrum of the product $U(\xi_1)/\{1+i\omega U(\xi_1)/[ev_{\max}(\xi_1)]\}^2$ was then computed for the frequencies between zero and 50 Hz with a step of 0.5 Hz and interpolated as a function of k_1 at each frequency. The value of the interpolated function was then taken at $k_1 = \omega(\cos\Psi/\beta-1/v)$ and plotted as a function of frequency, yielding the amplitude spectrum of the radiated shear wave.

Figure 2 presents the resulting distributions $U(\xi_1)$ along the fault for the cases when the minimum slip is zero and nonzero, as indicated by the labels. For comparison, the third scenario is added, in which the function τ in equation (18) was set to a constant average value, by assuming $U = 0.14$ m and $v_{\max} = 1$ m/s. The corner frequency in this case is constant

and equal to $f_c = ev_{max}/(2\pi U) = 3.1$ Hz. The third scenario hence is the one of the fault-position-independent shape function, described by equation (14) and represented by the black line in Figure 1a.

Figure 3 shows the resulting frequency spectra of radiation (the color coding of the scenarios corresponds to Fig. 2). Straight lines have been visually fitted to the high-frequency slopes; the frequency fall offs are $\omega^{-1.5}$, $\omega^{-2.6}$, and ω^{-4} for the cases of zero minimum slip (light gray line), nonzero one (dark gray line), and constant corner frequency (black line). Because of renormalization, the spectral units have switched to arbitrary. As seen, when the shape function $\Delta\dot{u}_s(t)$ is independent of the position on the fault (the case of constant τ), the spectrum reduces to the form of equation (14); the slope (power of ω) of −4 is thus expected (black line), as for the black lines in Figure 1 as well. The general case is however different and can be understood on physical grounds. In the product $F(\xi_1, \omega)$ in equation (19), the frequency spectrum $\Delta\dot{u}_s(\xi_1, \omega)$ has a variable corner frequency depending on ξ_1, controlled by equation (18) (the corner frequency is the inverse of τ). The slope of −2 in this spectrum is only present at frequencies above f_c. In the scenario of zero minimum slip, parts of the fault in which $U(\xi_1)$ is near zero radiate spectra with very large, nearly infinite corner frequency; in the seismic frequency range of Figure 3, these spectra are flat and contribute no additional slope, which causes the significant overall reduction of the frequency rolloff in the cumulative spectrum radiated by the entire fault (the light gray line in Fig. 3). On the other hand, there are no extremely high corner frequencies in the scenario of nonzero minimum slip; all parts of the fault contribute to the high-frequency decay, commensurate with their corner frequencies, and the fall-off rate expectedly becomes greater (the dark gray line in Fig. 3). The greatest negative slope for the k-square slip distribution is −4, which is achieved for the fault-position-independent temporal slip-rate function $\Delta\dot{u}_s(t)$.

A way to universally preserve the fall-off rates of ω^{-2} in the radiated spectrum in case of the variable slip-rate function, even if the latter executes its own low-pass filtering, was proposed by Bernard *et al.* (1996) and further investigated by Gallovič and Brokešová (2004). Such a preservation is achieved through an a priori postulation of an ad hoc inverse dependence of the rise time τ on the wavenumber in the large wavenumber range: $\tau = b/k_1$, in which b is a constant (Bernard *et al.*, 1996, their equation 13; Gallovič and Brokešová, 2004, their equation 5). Then the mechanism of retaining the slope of −2 is as follows. For $U(\xi_1)$ having a k-square spectrum (e.g., as in equation 21 or as used by Gallovič and Brokešová, 2004, their equation 6, as well as their equation 9 for the line source), substitution of $k_1 = \omega(\cos\Psi/\beta - 1/v)$ into it already provides an ω^{-2} term in the resulting radiation (e.g., as in equation 14). By the postulated assumption, if the spatially variable slip shape is a function of $\omega\tau$, as in equation (20), substitution of $k_1 = \omega(\cos\Psi/\beta - 1/v)$ into $\omega\tau = \omega b/k_1$ makes the frequency ω cancel and the resulting spatial spectrum $\Delta\dot{u}_s[\omega(\cos\Psi/\beta - 1/v)]$ frequency independent. If one could factorize $F[\omega(\cos\Psi/\beta - 1/v)]$ as $U[\omega(\cos\Psi/\beta - 1/v)]\Delta\dot{u}_s[\omega(\cos\Psi/\beta - 1/v)]$, that is, represent the Fourier transform of a product as the product of the Fourier transforms of the multipliers, then the only remaining dependence on frequency would come from $U[\omega(\cos\Psi/\beta - 1/v)]$, that is, would have the ω^{-2} shape.

Following this argument, any spatially variable temporal slip shape that is a function of $\omega\tau$ would always radiate the omega-square seismic spectrum. For example, the ramp function (the boxcar if expressed as slip velocity) falls in the same category (e.g., Aki and Richards, 1980, their equation 14.20), as used in the example of Bernard *et al.* (1996, their equations 10 and 17).

There are two issues with the proposed model. First, the assumed inverse dependence of the rise time on wavenumber does not have a reliable physical basis. Bernard *et al.* (1996, p. 1158) cautiously admit themselves that their hypothesis is "clearly speculative." Following the idea of decomposition of a function into the sinusoidal Fourier components (a Fourier series or Fourier transform), a function in space at any given point will generally simultaneously have contributions from many different harmonics, with both low and high values of k_1. Ambiguity in what harmonic to choose as the value of k_1 in assigning the rise time according to $\tau = b/k_1$ is clearly present.

Second, the Fourier transform of a product cannot be factorized into the product of two transforms (such an assumption is made by Gallovič and Brokešová, 2004, p. 212; it is also seen in equation 10 of Bernard *et al.*, 1996, developed for the boxcar slip-velocity function). Instead, as pointed out earlier, according to the convolution theorem (e.g., Båth, 1974, his section 3.2.2), the Fourier transform of a product is the convolution of the two transforms. For these reasons, the preservation of the omega-square spectrum of radiation by the assumption of the scale-dependent rise time is not a viable alternative.

CONCLUSIONS

Contrary to what is often assumed, the k-square slip distribution on fault ruptures produces the frequency spectra of body wave radiation that can have the fall-off rates as high as ω^{-4}. In the general case of the source time function that is dependent on the position on the fault, the rates can be highly variable in the approximate range of −1.5 and −4, depending on the specific k-square slip. The typical high-frequency decay rates in the observed seismic spectra are between one and three. The power-law rate of four is highly unusual, casting doubt on the suitability of certain k-square slip models as a prototype rupture scenario in earthquake hazard calculations, unless the appropriate heterogeneous slip distributions serve to supersede the ad hoc "f_{max}" or "kappa" high-cut filters as the source effect.

The spectrum of the source time function $\Delta u_s(\omega)$ is expected to exert primary control over the levels of high-frequency radiation from earthquakes (e.g., equations 4, 8, and 9), whereas the effects of random heterogeneity of fault's static slip are less significant (Beresnev, 2017a). For the temporal shape of slip in the form of the general ω^{-n} dislocation, the quantity τ (and thus ω_c) set the dislocation rise time. The high-frequency amplitudes are controlled by ω_c^{n+1} and hence by the quantity $v_{\max}^{n+1}$ (e.g., through equation 18 for $n = 2$) (Beresnev, 2019a, his equations 5, 6, and 8). The variability in $v_{\max}$ should thus be given careful consideration in the hazard models. The fact that the corner frequencies and the associated rise times should be chosen judiciously for the correct simulation of high-frequency radiation is underscored by Schmedes *et al.* (2013, p. 1129).

Two factors affecting the high-frequency slopes of seismic spectra have been examined in this article: the spectrum of the source time function and the distribution of static slip. As stated in the Introduction, the rupture speed has been assumed constant. As pointed out by Hisada (2000), spatial variations in this speed can introduce further modifications of high-frequency decay rates, although, as closely examined by Beresnev and Roxby (2021) and showed by Hisada (2000, his fig. 6a,b), the suppression of high frequencies occurs as an artifact of regular interference. It follows that a particular slope can be obtained in an ad hoc manner by constructing a specific timing of rupture travel. An example was provided by Hisada (2000), who modeled a line source with the fault-position-independent shape function $\Delta \dot{u}_s(t)$ represented by a combination of equilateral triangles (equations 16–18 in Hisada, 2000). Hisada (fig. 6a) tested three different rupture time models of variable degrees of randomness. The radiation was thus governed by the integral in our equation (9) with the time delay ξ_1/v in the integrand replaced by a spatially variable $\Delta t(\xi_1)$ (equation 23 in Hisada, 2000); this case was also investigated by Beresnev (2019b, his equation 6) and Beresnev and Roxby (2021, their equation 6). Out of the three travel time distributions tried by Hisada, only one possibility combined with the spatial distribution of slip and the triangle-type slip-velocity function to produce an ω-square radiated spectrum. A different choice of the travel time function would produce a different decay of the seismic spectrum.

It should be emphasized that equations (8), (9), (14), and (15), allowing simple interpretations of the modifications of the frequency spectra of the slip function by fault heterogeneity, are only valid for the underlying approximation of the body waves from a small source in the far field (equation 16). Such a limiting case serves illustrative purposes but is of no significant interest to earthquake hazard calculations. For the more practically important situation of the near field of a large earthquake source, the modification is described by the fault directivity spectrum $\mathbf{I}(\mathbf{x}, \omega)$ of complicated form (equations 2–4), even if the temporal shape $\Delta u_s(t)$ of the slip on the fault is assumed to be the same at all points. Simple conclusions about the effects of heterogeneous distributions of final fault slip on the resulting seismic spectra may no longer apply. A conclusion already reached is that purely random disturbances of slip do not significantly affect the finite-fault radiation described by the full equation (2) (Beresnev, 2017a). A comprehensive numerical study of the effect of other shapes of the spatial spectra of slip on finite planes is planned for the future.

DATA AND RESOURCES

No data were used in the article. All inferences were made through the analyses of the respective equations and literature sources as indicated.

DECLARATION OF COMPETING INTERESTS

The author acknowledges that there are no conflicts of interest recorded.

ACKNOWLEDGMENTS

The author is grateful to two anonymous referees for the comments on the article.

REFERENCES

Aki, K., and P. G. Richards (1980). *Quantitative Seismology*, W. H. Freeman and Company, San Francisco, California.

Båth, M. (1974). *Spectral Analysis in Geophysics*, Elsevier, Amsterdam, The Netherlands.

Beresnev, I. A. (2001). What we can and cannot learn about earthquake sources from the spectra of seismic waves, *Bull. Seismol. Soc. Am.* **91,** 397–400.

Beresnev, I. A. (2017a). Factors controlling high-frequency radiation from extended ruptures, *J. Seismol.* **21,** 1277–1284.

Beresnev, I. A. (2017b). Simulation of near-fault high-frequency ground motions from the representation theorem, *Pure Appl. Geophys.* **174,** 4021–4034.

Beresnev, I. A. (2019a). Interpretation of kappa and $f_{\max}$ filters as source effect, *Bull. Seismol. Soc. Am.* **109,** 822–826.

Beresnev, I. A. (2019b). Reply to "Comment on "Interpretation of kappa and $f_{\max}$ filters as source effect" by Igor A. Beresnev" by Arthur Frankel, *Bull. Seismol. Soc. Am.* **109,** 2764–2766.

Beresnev, I. A. (2021). The effects of variable velocity of rupture propagation on fault's directivity pulses, *Pure Appl. Geophys.* **178,** 3427–3439.

Beresnev, I. A., and G. M. Atkinson (1997). Modeling finite-fault radiation from the ω^n spectrum, *Bull. Seismol. Soc. Am.* **93,** 67–84.

Beresnev, I. A., and K. Roxby (2021). The effects of variable and constant rupture velocity on the generation of high-frequency radiation from earthquakes, *Pure Appl. Geophys.* **178,** 1157–1164.

Bernard, P., A. Herrero, and C. Berge (1996). Modeling directivity of heterogeneous earthquake ruptures, *Bull. Seismol. Soc. Am.* **86,** 1149–1160.

Boore, D. M. (2003). Simulation of ground motion using the stochastic method, *Pure Appl. Geophys.* **160,** 635–676.

Gallovič, F., and J. Brokešová (2004). On strong ground motion synthesis with k^{-2} slip distributions, *J. Seismol.* **8,** 211–224.

Graves, R., and A. Pitarka (2016). Kinematic ground-motion simulations on rough faults including effects of 3D stochastic velocity perturbations, *Bull. Seismol. Soc. Am.* **106,** 2136–2153.

Graves, R. W., and A. Pitarka (2010). Broadband ground-motion simulation using a hybrid approach, *Bull. Seismol. Soc. Am.* **100,** 2095–2123.

Graves, R. W., B. T. Aagaard, K. W. Hudnut, L. M. Star, J. P. Steward, and T. H. Jordan (2008). Broadband simulations for M_w 7.8 southern San Andreas earthquakes: Ground motion sensitivity to rupture speed, *Geophys. Res. Lett.* **35,** L22302, doi: 10.1029/2008GL035750.

Herrero, A., and P. Bernard (1994). A kinematic self-similar rupture process for earthquakes, *Bull. Seismol. Soc. Am.* **84,** 1216–1228.

Hisada, Y. (2000). A theoretical omega-square model considering the spatial variation in slip and rupture velocity, *Bull. Seismol. Soc. Am.* **90,** 387–400.

Infantino, M., I. Mazzieri, A. G. Özcebe, R. Paolucci, and M. Stupazzini (2020). 3D physics-based numerical simulations of ground motion in Istanbul from earthquakes along the Marmara segment of the north Anatolian fault, *Bull. Seismol. Soc. Am.* **110,** 2559–2576.

Mai, P. M., and G. C. Beroza (2002). A spatial random field model to characterize complexity in earthquake slip, *J. Geophys. Res.* **107,** 2308, doi: 10.1029/2001JB000588.

Razafindrakoto, H. N. T., F. Cotton, D. Bindi, M. Pilz, R. W. Graves, and S. Bora (2021). Regional calibration of hybrid ground-motion simulations in moderate seismicity areas: Application to the upper Rhine graben, *Bull. Seismol. Soc. Am.* **111,** 1422–1444.

Rodgers, A. J., N. A. Petersson, A. Pitarka, D. B. McCallen, B. Sjorreen, and N. Abrahamson (2019). Broadband (0-5 Hz) fully deterministic 3D ground-motion simulations of a magnitude 7.0 Hayward fault earthquake: Comparison with empirical ground-motion models and 3D path and site effects from source normalized intensities, *Seismol. Res. Lett.* **90,** 1268–1284.

Rodgers, A. J., A. Pitarka, R. Pankajakshan, B. Sjögreen, and N. A. Petersson (2020). Regional-scale 3D ground-motion simulations of M_w 7 earthquakes on the Hayward fault, northern California resolving frequencies 0-10 Hz and including site-response corrections, *Bull. Seismol. Soc. Am.* **110,** 2862–2881.

Ruiz, J. A., D. Baumont, P. Bernard, and C. Berge-Thierry (2011). Modelling directivity of strong ground motion with a fractal, k^{-2}, kinematic source model, *Geophys. J. Int.* **186,** 226–244.

Schmedes, J., R. J. Archuleta, and D. Lavallée (2013). A kinematic rupture model generator incorporating spatial interdependency of earthquake source parameters, *Geophys. J. Int.* **192,** 1116–1131.

Somerville, P., K. Irikura, R. Graves, S. Sawada, D. Wald, N. Abrahamson, Y. Iwasaki, T. Kagawa, N. Smith, and A. Kowada (1999). Characterizing crustal earthquake slip models for the prediction of strong ground motion, *Seismol. Res. Lett.* **70,** 59–80.

Wells, D. L., and K. J. Coppersmith (1994). New empirical relationships among magnitude, rupture length, rupture width, rupture area, and surface displacement, *Bull. Seismol. Soc. Am.* **84,** 974–1002.

Manuscript received 27 August 2021
Published online 2 March 2022